USC–SIPI REPORT #242

Signal Modeling with Extended Self-Similar Processes

by

Lance M. Kaplan and C.-C. Jay Kuo

September 1993

Signal and Image Processing Institute
UNIVERSITY OF SOUTHERN CALIFORNIA
Department of Electrical Engineering-Systems
3740 McClintock Avenue, Room 404
Los Angeles, CA 90089-2564 U.S.A.

Signal Modeling with Extended Self-Similar Processes*

Lance M. Kaplan† and C.-C. Jay Kuo†

September 13, 1993

EDICS: SP 2.7.6

Abstract

The fractional Brownian motion (fBm) model has proven to be valuable in modeling many natural processes because of its self-similarity character. However, the model is characterized by one single parameter which cannot distinguish between short and long term correlation effects. This work investigates the idea of generalizing self-similarity to create extended self-similar (ESS) processes for which fBm processes are a subset. Properties of ESS processes are discussed and examples are provided. Additionally, an ESS increment model parameterized by variables controlling short and long term correlation effects is examined. We derive a theorem about the variance progression of the output coefficients of the Haar transform applied to the ESS increments and justify the "whitening" effect of the Haar transform applied to decaying stationary processes. These results lead to a fast parameter estimation algorithm for ESS processes. We demonstrate the performance of this parameter estimation algorithm with numerical simulations.

1 Introduction

Many natural processes such as the cross section of a mountain range, weather data, electrical measurements and even man made phenomena such as economic and traffic flow data have been observed to follow the $1/f$ law [17], [25]. The fractional Brownian motion (fBm) processes are important because the spectrum of an fBm follows a $1/f$ power law which means that fBm provides a correlation model for $1/f$ processes. The traditional Markov process has fast correlation decay which translates into the fact that it provides too little energy in the low frequency range of the spectrum to model the natural $1/f$ effect. One characterizing feature of fBm is its statistical self-similar property [22]. By statistical self-similarity, we mean that the variance of increments of a

*This work was supported by a National Science Foundation Fellowship and the National Science Foundation Young Investigator (NYI) Award ASC-9258396 and the Presidential Faculty Fellow (PFF) Award GER 93-50309.

†The authors are with the Signal and Image Processing Institute and the Department of Electrical Engineering-Systems, University of Southern California, Los Angeles, California 90089-2564. E-mail: lancekap@sipi.usc.edu and cckuo@sipi.usc.edu.

process obeys a hyperbolic scaling law so that the statistical properties of the process at any two scales are the same within a scaling constant.

The fBm model is frequently used in computer graphics for synthesis of naturally looking curves and images. Each realization of fBm is a fractal [21] and the roughness of the fBm realization is invariant to scale. Various variants of the fBm model have also been studied and applied. In many cases, textures and natural data are modeled by the increments of the sampled fBm, also known as discrete fractional Gaussian noise (dfGn), instead of fBm itself. Another model known as fractionally differenced Gaussian noise (fdGn) was introduced in [10], [12]. It has the same long term correlation decay characteristics as dfGn, but is easier to use since closed form solutions to the reflection coefficients exist for fdGn [4], [12]. The fBm, dfGn, and fdGn models, or simply fractal models, have been successfully applied to texture analysis and synthesis [16], [26] and landscape modeling [25]. Texture classification algorithms were developed for medical applications [2], [20]. Texture segmentation algorithms based on fractal models were presented in [11], [15], [26]. Moreover, a fractal dimension estimator was used for speech segmentation [5].

Despite many existing fractal models, they are limited in the sense that they are only characterized by a single parameter and not versatile enough to model short term effects. In contrast, the traditional ARMA model has an indefinite number of parameters to shape the correlation function, but it has difficulty in representing stochastic signals with slow decaying correlation [12]. For instance, given a p^{th} order AR model to represent the correlation of an dfGn, the first p terms of the correlation function for the AR model will decay hyperbolically matching the dfGn terms, but the remaining terms will decay exponentially. In an effort to design stationary correlation models that handle both short and long term correlations, Hosking proposed to consider filtered fractals such that fractionally differenced Gaussian noise (fdGn) is passed through a rational (i.e. ARMA) filter. Note that the long term behavior of fdGn is the same as dfGn. Deriche and Tewfik have implemented a maximum likelihood technique to estimate the parameters of the fdGn process and the ARMA filter [5]. The algorithm, however, is computationally extensive.

While it makes sense to think of natural textures as being self-similar over a large range of scales, it is unreasonable to think that the self-similarity continues to infinitesimal scales. For instance, the concept of the atom ended a long debate that one could cut any object into arbitrarily smaller pieces where each piece has the same characteristics as the original object. In fact, natural processes are shaped by physics, where the behavior of large bodies is very different from that of small ones (governed by quantum mechanics). Some shortcomings of the fBm model for realism of natural scenery in the application of computer graphics were discussed by Lewis [18].

These shortcomings motivate us to extend the idea of self-similarity such that the variance of the increments of a process is related to a certain function of scale, i.e. the growth function, and we call the resulting processes the extended self-similar (ESS) processes. The growth function has to satisfy a certain set of properties so that the ESS processes are mean squared continuous and have proper correlation functions. We give examples of different growth functions and their associated ESS processes. In most cases, ESS processes are not strictly self-similar in the sense that their statistics may vary with scales. To show the application of ESS processes, we consider a ESS-based model that has one parameter to control the short term correlation and another parameter to control the long term correlation of a random signal. Besides, we derive a theorem about how the variance progression of the output coefficients of the Haar transform applied to the ESS increments is related to sampled values of the growth function, and we justify the "whitening" effect of the Haar transform applied to decaying stationary processes. The theorem leads to a fast parameter estimation algorithm which is essential to signal modeling with the ESS model, and the theorem also demonstrates that the growth function provides a measure of how the frequency content of a signal changes with scale. Through some examples, it will be shown that adding short term correlations into the growth functions will smooth out ESS realizations for smaller scales. In other words, manipulation of the growth function can change the visual roughness of a ESS realization at various scales. Furthermore, because one can create growth function parameterized to measure different correlation effects, the new ESS concepts should be useful for synthesis, classification, and segmentation of signals, textures or landscapes.

This paper is organized as follows. Theory of fBm is presented in Section 2, and theoretical properties of ESS processes appear in Section 3. Section 4 shows how the ESS processes are useful for signal modeling, and introduces a parameter estimation algorithm for stationary signals. Finally, Section 5 concludes the paper.

2 Fractional Brownian Motion

Properties of fBm have been examined by many researchers, say, [6], [7], [14], [22], [25], [27], [30], and [32]. We will review some basic results of fBm in this section. By definition, fBm is a zero-mean Gaussian random process such that each realization $B_H(t)$ satisfies

$$B_H(t) = 0, \tag{2.1}$$

and the self-similarity condition

$$\mathrm{VAR}(B_H(s+p) - B_H(s)) = |p|^{2H}\mathrm{VAR}(B_H(t+1) - B_H(t)) = |p|^{2H}\sigma^2, \tag{2.2}$$

where VAR denotes the variance and $0 < H < 1$ is known as the Hurst parameter. The bounds on H assure that the fBm process is mean squared continuous and that the correlation function possesses the properties of an inner product [22]. The self-similarity condition leads to the fact that the realizations of fBm are fractals with a fractal dimension of [21]

$$D = 2 - H.$$

Thus, the Hurst parameter controls the "roughness" of fBm. Based on (2.1) and (2.2), the correlation function of $B_H(t)$ can be derived as

$$r_{B_H}(s,t) = \frac{\sigma^2}{2}(|s|^{2H} + |t|^{2H} + |s-t|^{2H}). \tag{2.3}$$

Equation (2.3) shows that fBm is a nonstationary process, and if $H = 1/2$, the fBm process has the correlation structure of normal Brownian motion. Moreover, a Brownian motion realization can be filtered to generate fBm by calculating the following integral [22],

$$\begin{aligned} B_H(0) &= 0, \\ B_H(t) &= \frac{1}{\Gamma(H+\frac{1}{2})}\left\{\int_{-\infty}^{0}[(t-s)^{H-1/2} - (-s)^{H-1/2}]dB(s) + \int_0^t (t-s)^{H-1/2}dB(s)\right\}. \end{aligned}$$

In fact, the above integral provides an alternative definition of fBm which was used in [22] where the self-similarity property is a characteristic of the resulting fBm process.

In many cases, only a finite set of discrete fBm data samples are available, and one would consider fBm sampled in intervals of Δx. The increment

$$X_H(k, \Delta x) = B_H(\Delta x(k+1)) - B(\Delta x k), \quad k \in \mathbf{Z}, \tag{2.4}$$

defines a sequence known as discrete fractional Gaussian noise (dfGn). It is easy to see that dfGn of incremental length Δx is a stationary process with the correlation function

$$r_{X_H}(k; \Delta x) = \frac{\sigma^2}{2}|\Delta x|^{2H}(|k+1|^{2H} + |k-1|^{2H} - 2|k|^{2H}). \tag{2.5}$$

FBm can be divided into three categories: (1) $0 < H < 1/2$ where the increments are negatively correlated, (2) $H = 1/2$ where the increments are uncorrelated (i.e. Brownian motion), and (3) $1/2 < H < 1$ where the increments are positively correlated.

Although fBm is nonstationary and thus has no formal power spectrum, Flandrin [6] has shown that the "average" spectrum follows a $1/f$ law as

$$S_{B_H}(\omega) \propto \frac{1}{|\omega|^{2H+1}}.$$

The dfGn process does have a proper power spectrum which is

$$S(e^{j\omega}) = r_{X_H}(0;\Delta x) + 2\sum_{k=1}^{\infty} r_{X_H}(k;\Delta x)\cos(\omega k). \tag{2.6}$$

This series is guaranteed to converge for $\omega \in (0,\pi]$ by the general alternating series theorem [28]. At $\omega = 0$,

$$S_{X_H}(e^{j0}) = \begin{cases} 0, & 0 < H < 1/2, \\ \sigma^2|\Delta x|^{2H}, & H = 1/2, \\ \infty, & 1/2 < H < 1. \end{cases} \tag{2.7}$$

The power spectrum can be expressed in another way by considering continuous increments (i.e. $X_H(t;\Delta x) = B(t+\Delta x) - B(t)$ for $t \in \mathbf{R}$) so that the correlation function is

$$r_{X_H}(t;\Delta x) = \frac{\sigma^2}{2}(|t+\Delta x|^{2H} + |t-\Delta x|^{2H} - 2|t|^{2H}) \quad t \in \mathbf{R}. \tag{2.8}$$

Then, based on the following result in [9],

$$2\int_0^{\infty} x^{v-1}e^{-ax}\cos(\omega x)dx = \Gamma(v)(a^2+\omega^2)^{-v/2}\cos(v\arctan(\frac{\omega}{a})), \tag{2.9}$$

where $\Re(a) > 0$, $\Re(v) > 0$, and $\omega > 0$, one can take the limit as $a \to 0$ and set $v = 2H+1$ to see that the continuous Fourier transform of (2.8) converges pointwise to

$$S_{X_H}(\omega) = 4\Gamma(2H+1)\sin(\pi H)\sigma^2\frac{\sin^2(\Delta x\frac{\omega}{2})}{\omega^{2H+1}}. \tag{2.10}$$

This expression is similar to a result in [6] except that the proper coefficients are included in (2.10). Finally, sampling (2.8) every Δx unit to obtain (2.5) will lead to aliasing of (2.10) so that the power spectrum of dfGn is

$$S_{X_H}(e^{j\omega}) = 4\Gamma(2H+1)\sin(\pi H)\sigma^2|\Delta x|^{2H}\sin^2(\frac{\omega}{2})\sum_{i=0}^{\infty}\left[\frac{1}{(\omega+2\pi i)^{2H+1}} + \frac{1}{(-\omega+2\pi(i+1))^{2H+1}}\right]. \tag{2.11}$$

The series will converge for $H > 0$ since the terms of the sequence converge to zero faster than $1/n$ [28].

Equations (2.6) and (2.11) provide two alternative methods to estimate the power spectrum of dfGn. Both equations demonstrate the self-similarity of fBm by the fact that the statistics of the

increments of fBm of different incremental lengths (i.e. Δx) are identical within a scaling factor of $|\Delta x|^{2H}$. The shape of the power spectrum is important for analysis, and the following theorem is helpful.

Theorem 1 *Given that $S(e^{j\omega})$ is the power spectrum of a dfGn process, then for $\omega \in (0, \pi]$, $S(e^{j\omega})$ is constant if $H = 1/2$, $S(e^{j\omega})$ is increasing if $0 < H < 1/2$, and $S(e^{j\omega})$ is decreasing if $1/2 < H < 1$.*

Since the dfGn derived from Brownian motion (i.e. $H = 1/2$) is white, the first statement of the theorem is trivial. The other statements are proved in Appendix A.1. By (2.7) and Theorem 1, if $1/2 < H < 1$, then the power spectrum of dfGn has an unbounded maximum at $\omega = 0$ and a minimum value at $\omega = \pi$, and if $0 < H < 1/2$, then the power spectrum of dfGn has a minimum value of 0 at $\omega = 0$ and a maximum value at $\omega = \pi$.

We also plot the power spectrum at $\omega = \pi$ as a function of H (with $|\Delta x| = 1$ and $\sigma^2 = 1$) in Fig. 1 by using (2.6) and (2.11). Note that for smaller values of H, the convergence of (2.11) is very slow and increasing the number of samples to sum over will cause the bottom curve in Fig. 1 to converge to the top curve. Fig. 1 also shows that

$$S_{X_H}(e^{j\pi}) \approx 2 - 2H. \tag{2.12}$$

Equation (2.12) will be useful for creating positive definite signal models that are asymptotically dfGn (See Appendix A.3).

3 Extended Self Similarity

FBm has proven to be a very a useful model, but the model is limited since only one parameter controls the shape of the spectrum of fBm. By extending the notion of self-similarity, a more general class of nonstationary correlation models can be generated which have stationary increments. These new models will also provide insights into methods to modify the shape of the fBm spectrum in the higher frequency region.

3.1 Definition and Properties

An extended self-similar (ESS) process is a zero mean Gaussian process such that given a realization of the process $B_f(t)$, then

$$B_f(0) = 0, \tag{3.1}$$

and the process has the extended self-similar property that

$$\mathrm{VAR}(B_f(s+p) - B_f(s)) = f(p)\mathrm{VAR}(B_f(t+1) - B_f(t)) = f(p)\sigma^2. \tag{3.2}$$

The function $f(p)$ will be referred to as the *growth function* since it reflects the growth of the variance of increments of a process as the incremental length (or scale) increases. The growth function must satisfy some conditions to be discussed in this section. Note that the incremental length Δx is related to the scale m by $\Delta x = C2^m$, where $m = 0, 1, 2, \ldots$ and C can be any positive real number. This notion of scale is consistent with the notion of scale in wavelet analysis.

Analogous to the derivation of the correlation structure of fBm, we can use (3.1) and (3.2) to determine the correlation of the process $B_f(t)$ as

$$r_{B_f}(s,t) = \frac{\sigma^2}{2}[f(s) + f(t) - f(s-t)], \quad s,t \in \mathbf{R}. \tag{3.3}$$

The increments of the ESS process,

$$X_f(k;\Delta x) = B_f(\Delta x(k+1)) - B_f(\Delta x k), \quad k \in \mathbf{Z},$$

are stationary and have the correlation function

$$r_{X_f}(k;\Delta x) = \frac{\sigma^2}{2}[f(\Delta x(k+1)) + f(\Delta x(k-1)) - 2f(\Delta x k)], \quad k \in \mathbf{Z}. \tag{3.4}$$

Note that the shape of the correlation function in (3.4) would be invariant to the incremental length if

$$f(ab) = f(a)f(b). \tag{3.5}$$

This property leads to true self-similarity. The only measurable functions to satisfy (3.5) have the form $f(p) = |p|^{2H}$ [22]. Therefore, fBm is the only true self-similar process in the class of ESS processes.

We require the growth function $f(p)$ to satisfy the following three conditions:

C1: $f(1) = 1$.

C2: $f(0) = \lim_{p \to 0} f(p) = 0$.

C3: The $r_{B_f}(s,t)$ given by (3.3) is a well defined correlation function.

The first condition is necessary for (3.2) to be consistent, and the second condition is needed for ESS processes to be mean squared continuous.

Since the positive definite property of correlation functions is in general difficult to verify, the third condition is not easy to check. An alternative condition is that $r_{X_f}(k, \Delta x)$ given in (3.4) is well defined as Δx goes to zero. This alternative condition is easier to check since the increments are stationary and one can see whether the power spectrum of the increments is positive. The third condition also leads to a set of necessary conditions of the growth function which are useful for quick analysis. These conditions are:

1. Positivity
$$f(p) \geq 0,$$
2. Symmetry
$$f(p) = f(-p),$$
3. Minkowski
$$f^{1/2}(s+t) \leq f^{1/2}(s) + f^{1/2}(t).$$

These conditions are necessary to insure that the correlation functions in (3.3) and (3.4) have the properties of an inner product.

It is important to understand how a set of growth functions can be manipulated to create other valid growth functions. In fact, given a set of growth functions, other valid growth functions can be generated by taking weighted averages as the following theorem states.

Theorem 2 *Given a finite set of valid growth functions,* $\{f_i(p) : i = 1, \ldots, N\}$, *and a set of positive coefficients,* $\{a_i : i = 1, \ldots, N\}$ *where*

$$\sum_{i=1}^{N} a_i = 1,$$

then

$$f(p) = \sum_{i=1}^{N} a_i f_i(p)$$

is a valid growth function.

Proof: Since $f_i(p)$ are valid growth functions,

$$f(1) = \sum_{i=1}^{N} a_i f_i(1) = \sum_{i=1}^{N} a_i = 1.$$

Also,

$$f(0) = \sum_{i=1}^{N} a_i f(0) = 0,$$

$$\lim_{s \to 0} f(s) = \sum_{i=1}^{N} a_i \lim_{s \to 0} f(s) = 0 = f(0).$$

Finally, the correlation function of the ESS process by (3.3) yields

$$r_f(s,t) = \sum_{i=1}^{N} a_i r_{f_i}(s,t),$$

where the corresponding finite set of correlation functions $r_{f_i}(s,t)$ defined by (3.3) are a set of well defined correlation function. Therefore, $r_f(s,t)$ is a proper correlation function. □

3.2 Discrete Haar Transform

The continuous wavelet transform (CWT) of processes with stationary increments was studied in [23], and the results apply to ESS processes. The wavelet transform coefficients of ESS processes are well defined, and the detail wavelet coefficients are stationary within scale. In practice, one might not be able to compute the CWT. Thus, a study of the discrete Haar transform on ESS increments is helpful and the results will be applied to an estimation algorithm in Section 4. The discrete Haar transform provides a multiresolution decomposition of a discrete data sequence. Given the data sequence $a_0(k)$ (i.e. the finest scale approximation to the continuous signal), the higher scale approximation coefficients $a_m(k)$ and detail wavelet coefficients $d_m(k)$ of the Haar transform are computed recursively by

$$a_{m+1}(k) = \frac{1}{\sqrt{2}}(a_m(2k) + a_m(2k+1)), \tag{3.6}$$

$$d_{m+1}(k) = \frac{1}{\sqrt{2}}(a_m(2k) - a_m(2k+1)). \tag{3.7}$$

When the increments of an ESS process is put through the discrete Haar transform, the extended self-similarity property provides simple expressions of the correlation of the approximation and detail wavelet coefficients using the growth function as stated in the following theorem.

Theorem 3 *Let $B_f(k)$ be a realization of an ESS process with incremental length Δx, and $a_0(k)$ be the finest scale approximation of the increments of $B_f(k)$. Define the stochastic processes $a_m(k)$ and $d_m(k)$ to be the approximation and detail wavelet coefficients, respectively, of the Haar transform as given in (3.6) and (3.7). Then,*

(a) for fixed scale m, the correlation of $a_m(k)$ is

$$r_{a_m}(k) = 2^{-m} r_{X_f}(k; 2^m \Delta x), \tag{3.8}$$

where $r_{X_f}(k)$ is given in (3.4);

(b) for fixed scale m, $d_m(k)$ is stationary and the variance of $d_m(k)$ is

$$\sigma_m^2 = r_{d_m}(0) = \sigma^2 2^{-m}(4f(2^{m-1}\Delta x) - f(2^m \Delta x)). \tag{3.9}$$

Proof: Since $a_0(k) = X_f(k; \Delta x)$, it is easy to see through (3.6) that

$$\begin{aligned} a_m(k) &= 2^{-m/2} \sum_{i=0}^{2^m-1} X_f(2^m k + i; \Delta x) \\ &= 2^{-m/2} X_f(k; 2^m \Delta x), \end{aligned}$$

and (3.8) follows. The stationarity of $d_m(k)$ is due to the fact that the process is derived by passing the stationary process $a_{m-1}(k)$ trough a linear filter. Then, (3.7) and (3.8) implies

$$r_{d_m}(k) = 2^{-m}(2r_{X_f}(2k; 2^{m-1}\Delta x) - r_{X_f}(2k+1; 2^{m-1}\Delta x) - r_{X_f}(2k-1; 2^{m-1}\Delta x)).$$

By setting $k = 0$ and using (3.4) then (3.9) follows. □

For the special case that the growth function is $|p|^{2H}$ (i.e. the fBm process), equation (3.9) leads to the following corollary which was used in [14] for the design of a fractal estimation algorithm.

Corollary 1 *Let $d_m(k)$ be defined as in Theorem 3 where $a_0(k)$ is the increments of fBm of incremental length Δx. Then,*

$$r_{d_m}(0) = 2^{(2H-1)(m-1)} \sigma^2 |\Delta x|^{2H} (2 - 2^{2H-1}).$$

The Haar transform can also effectively decorrelate ESS increments whose correlation is decaying over time. A technique originated in [24] and used by Tewfik and Kim in [29] can verify that the detail wavelet coefficients of the Haar transform will have a correlation structure that decays faster than the original ESS increments as long as the correlation of the stationary ESS increments decay over time. In other words, the Haar transform effectively whitens ESS increments. Specifically, when the correlation structure of (3.4) is treated as a continuous function, then the function will be continuously differentiable if the growth function is continuously differentiable. Based on [29], it can be argued that if a Daubechies filter of length $2R$ [3] is used for discrete wavelet transform (DWT)

implementation ($R = 1$ for the Haar transform), the correlation of detail wavelet coefficients is bounded by

$$E[d_m[k]d_n[l]] \leq \sup_{0 \leq k',l' < 2R} \left| \frac{d^{2R} r[t]}{dt^{2R}} \right|_{t=2^m k - 2^n l - k' + l'}. \tag{3.10}$$

If the growth function leads to increments which have some terms decaying exponentially and other terms decaying hyperbolically (e.g. fBm), the correlation of detail wavelet coefficients decay faster than that of original ESS increments because of (3.10). The faster decay for the exponential terms is due to the larger sampling period at higher scales while the faster convergence of the hyperbolic terms was verified in [14]. Section 4.1 will verify the "whitening" effect of the Haar transform on increments of ESS processes with correlation decay. While there is decay in correlation of wavelet coefficients as the time domain overlap decreases, there is, however, some significant correlation between coefficients of different scales having overlapping temporal support. As a result, the correlation structure of the stationary wavelet coefficients is usually banded. Examples of the banded structure will also be presented in Section 4.1.

3.3 Examples

Many growth functions can be used to generate different ESS processes. This section will look at three examples of growth functions and report their implications.

Example 1: Hyperbolic function

The hyperbolic growth function of the form $f_H(p) = |p|^{2H}$ leads to fBm where the Hurst parameter controls the roughness of the process. The properties of fBm have been reviewed in Section 2. The important characteristic of fBm is that it is truly self-similar. Fig. 2 shows an fBm realization with $H = .65$ at scales $m = 4$ and $m = 0$, where scale m means the process is sampled every 2^m units. Note that the finer scale is normalized as in [25] by a factor of 2^{Hm} so that the statistics of the process at the two scales match. The self-similarity of fBm is evident as the realization at the two different scales appears to have the same roughness.

Example 2: Sinusoidal function

The sinusoidal ESS process is a processes such that the variance of a point of the process is bounded which is a large contrast to fBm. The growth function of such a process is

$$f_\omega(p) = \frac{\sin^2(\omega p)}{\sin^2(\omega)},$$

and the correlation function of the increments of incremental length Δx is

$$r_{f_\omega}(k; \Delta x) = \sigma^2 \frac{\sin^2(\omega \Delta x)}{\sin^2(\omega)} \cos(2\omega \Delta x k).$$

Since $r_{f_s}(k;\Delta x)$ is well defined for all Δx, the growth function is valid. The correlation of the actual ESS process $B_\omega(t)$ is

$$r_{B_\omega}(s,t) = \frac{\sin(\omega s)\sin(\omega t)}{\sin^2\omega}\cos(\omega(s-t)).$$

Some realizations of a sinusoidal ESS for $\omega = \pi/15$ at scales $m = 3$ and $m = 0$ in Fig. 3. The increments of the sinusoidal ESS at any Δx give rise to a rank two process [31] (i.e. the KL expansion has just two terms). As a result, viewing the ESS realizations at different scales does not provide any new information about the randomness of the process. The difference between the realization at the two scales in Fig. 3 is a matter of sampling. We may conclude that the sinusoidal ESS has little random information so that it has no roughness or natural texture component as seen in Fig. 3.

Example 3: Exponential function

The exponential growth function leads to increments that have quickly decaying correlation structure. As a result, at large scales the corresponding process will appear as rough as Brownian motion. The growth function

$$f_\rho(s) = \frac{2\rho}{(1-\rho)^2}(\rho^{|s|}-1) + \frac{1+\rho}{1-\rho}|s|, \quad 0 \le \rho < 1, \tag{3.11}$$

generates a well defined process as shown in Appendix A.2. The second linear term of (3.11) exists to regularize the exponential decay so that the growth function is valid. In fact, the increments at a sampling period $\Delta x = 1$ have a correlation function of

$$r_{f_\rho}(k) = \sigma^2\rho^{|k|}.$$

Therefore, the increment process is equivalent to an AR(1) process for $0 \le \rho < 1$. By looking at (3.11), one can see that the first term represents the short term decay whose significance disappears as s becomes large while the second term represents Brownian motion (i.e. fBm with $H = 1/2$). This means that the correlation structure of the increments of the ESS quickly go to zero since the increments are asymptotically white, and at large scales the ESS process converges to Brownian motion. Fig. 4 shows the exponential ESS process at scales $m = 4$ and $m = 0$ where the finer scale values are scaled by a factor of $\sqrt{2}$ using the scaling concept of fBm presented in [25]. One can see that the process is smoother at the finer scale.

3.4 Discrete Processes

When processing signals through the computer, one can only consider a finite discrete set of data samples, Thus, one need to use discrete correlation models. The ESS model provides a continuous

model which can be sampled at intervals of Δx so that one only needs to know the correlation at integer multiples of Δx. By considering sampled ESS processes, the increments with incremental length Δx are the finest resolution increments available and serve as the stationary building block of the sampled ESS process. For convenience, we will set $\Delta x = 1$ when discussing sampled ESS processes. A natural question to ask is what type of stationary processes can be used as the finest scale increments of an ESS process. The answer is that any stationary process can constitute increments because summing the stationary processes $X(k)$, i.e.

$$B(k) = \sum_{i=0}^{k-1} X(i), \quad k = 0, 1, 2, \ldots$$

will create a nonstationary process with a well defined correlation function.

The growth function associated with a sampled ESS process turns out to be a sampled function defined on integer values, and can be calculated by the correlation function of the stationary increments as stated in the following theorem.

Theorem 4 *Let $X(k)$ be the finest scale increments of a sampled ESS process. Then, the growth function of the ESS process is given by*

$$f(p) = f(p-1) + 1 + \frac{2}{r(0)} \sum_{k=1}^{p-1} r(k), \quad p = 2, 3, \ldots \tag{3.12}$$

or

$$f(p) = p + \frac{2}{r(0)} \sum_{k=1}^{p-1} (p-k) r(k), \quad p = 2, 3, \ldots \tag{3.13}$$

where $f(0) = 0$, $f(1) = 1$, and $f(-p) = f(p)$.

Proof: Since $r(0)$ represents the variance of the finest incremental length, the variance of the increments of incremental length p is $r(0)f(p)$ by (3.2), i.e.

$$r(0)f(p) = \mathrm{VAR}\left(\sum_{i=0}^{p-1} X(pk+i) \right),$$

and (3.13) follows. Then, by considering $f(p) - f(p-1)$, (3.12) follows. □

The growth function provides a tool to analyze the structure of correlation functions, and was actually estimated in [11] to create a suboptimal estimator for the Hurst parameter. The form of a long correlation model is much easier to study by examining the growth function rather than the correlation function. The Haar transform and other wavelet transforms in a sense provide estimates of the growth function at different scales (e.g. dyadic points on the growth function). The growth

function also provides a new tool for synthesis since one can create a growth functions so that the increments of a sampled ESS process has varying roughness for various incremental length or scale. Finally, the growth function will allow to create models that are asymptotically fBm for large scales, but with short-term correlations added for smaller scales.

3.5 2D and Higher Dimensional ESS processes

For 2-D texture analysis and synthesis, 1-D ESS processes as defined by (3.2) have to be generalized. It is straightforward to define ESS processes on a n-dimensional lattice. That is, the self-similarity condition on the lattice $\mathbf{R}^n$ can be written as

$$\mathrm{VAR}(B_f(\vec{s}+\vec{p}) - B_f(\vec{s})) = f(\|\vec{p}\|)\mathrm{VAR}(B_f(\vec{t}+\vec{1}) - B_f(\vec{t})) = f(\|\vec{p}\|)\sigma^2,$$

where $\|\cdot\|$ is any norm for $\mathbf{R}^n$ and $\|\vec{1}\| = 1$. For most case, it is natural to choose the normal 2-norm on $\mathbf{R}^n$. The correlation function of the n-D ESS process is simply

$$r_{B_f}(\vec{s},\vec{t}) = \frac{\sigma^2}{2}(f(\|\vec{s}\|) + f(\|\vec{t}\|) - f(\|\vec{s}-\vec{t}\|)).$$

The ESS process is isotropic with respect to the chosen norm, and any 1-D slice of the process produces a 1-D process whose statistics are determined by the same growth function. Therefore, one can apply the concept of ESS processes to synthesize a broader class of textures and landscapes than fBm.

4 Signal Modeling

DfGn serves a good model for stationary processes with significant long term correlations, but only one parameter controls the shape of the correlation function for fBm increments. We propose to use the growth function to create a model that has one parameter that controls the short term effects and another parameter for long term effects in this section. A numerically simple estimation algorithm is proposed and tested in numerical simulations.

4.1 Asymptotic fBm

The goal is to find a model whose correlation decays asymptotically like a fractal, but where the short term correlations differ from the normal dfGn model. Equation (3.11) provides a correlation model that decays in the long term as white noise (i.e. dfGn for $H = 1/2$). In fact, the second term of (3.11) generates the white noise, while the significance of the first term is exponentially

decaying. The coefficients of the terms in (3.11) are balanced so that the finest scale increments with $\Delta x = 1$ have the decay of an AR(1) process. Therefore, it is logical to replace the white noise generating second term to a term that generates dfGn for $1/2 < H < 1$ while choosing carefully the coefficients of the two terms so that the resulting growth function creates a positive definite correlation function. (It is worthwhile to comment that dfGn for $0 < H < 1/2$ is a different process than dfGn for $1/2 < H < 1$, and that we find it difficult to expand the dfGn for the two processes into the same extended model). One such growth function is

$$f(s) = \frac{A-1}{1-|\rho|}(|\rho|^{|s|} - 1) + A|s|^{2H}, \tag{4.1}$$

where

$$A = \frac{2H + \rho(2-2H)}{2H - \rho(2-2H)}, \quad 1/2 < H < 1, \ -1 < \rho < G(H). \tag{4.2}$$

We show that the growth function is valid for discrete ESS processes with the finest increment $\Delta x = 1$ and discuss the determination of the bound $G(H)$ on ρ in Appendix A.3. A plot of $G(H)$ is given in Fig. 5. Note that (4.1) does not provides a valid continuous ESS process because as s goes to zero, $f(s)$ violate the positivity condition.

The resulting correlation function of the finest scale increments by (3.4) is

$$r_f(k) = \begin{cases} \sigma^2, & k = 0, \\ \frac{\sigma^2}{2}\left[(A-1)(1-|\rho|)|\rho|^{k-1} + A(|k+1|^{2H} + |k-1|^{2H} - 2|k|^{2H})\right], & k = 1, 2, \ldots \end{cases} \tag{4.3}$$

The corresponding ESS increment model is called the *asymptotic dfGn* (adfGn). The shape of the adfGn model is controlled by two parameters where ρ provides a transient correlation effect while H introduces the long term fractal structure. The coefficient A is chosen so that when $\rho = 0$, the model is simply dfGn, and when $H = 1/2$, the growth function is (3.11) which provides AR(1) increments. Moreover, the corresponding nonstationary discrete ESS model is asymptotically fractal for coarse scales, and will be referred to as asymptotic fBm (afBm). The parameter ρ will smooth out the finer scales, and the parameter H controls the roughness of the process at coarser scales. Fig. 6 demonstrates how adfGn expands upon AR(1) and dfGn models by showing the correlation function for various values of ρ and H when the $\sigma^2 = 1$ and the correlations at lag one are equal. Plots of afBm at scales $m = 4$ and $m = 0$ are shown in Fig. 7 with $\rho = 0.85$ and $H = 0.65$. Note that the realization at different scales is scaled in a similar way as in [25] according to the H parameter which represents the asymptotic fractal structure. It is evident that the afBm realization is smoother at finer scales, while at coarser scales the process is as rough as the fBm with the same value of H.

The correlation decay of adfGn is evident in (4.3). It is represented by an exponentially decaying term along with a hyperbolically decaying term. As discussed in Section 3.2, the Haar transform

can effectively whiten the stationary adfGn process when there is no temporal overlap of the wavelet coefficients. For instance, we show the correlation of an adfGn process of length 64 with $\rho = 0.5$ and $H = 0.75$ in Fig. 8. The theoretical correlation matrix of the detail wavelet coefficients of the process is given in Fig. 9. An experimental correlation matrix was calculated by generating 256 samples of the adfGn and averaging over the calculated correlation of the resulting Haar coefficients, we show the the experimental matrix in Fig. 10. We see clearly from Figs. 9 and 10 the banded correlation structure resulting from the wavelet transform. Besides, there exist strong main diagonals so that the "whitening" assumption of the Haar transform is approximately valid.

4.2 Parameter Estimation

This section will discuss a parameter estimation algorithm that generalizes the class of fBm estimation algorithms by considering the adfGn model. The estimation of the fractal dimension of an fBm realization has proven to be an important problem for signal and image analysis. Traditional techniques are based on some type of regression analysis to measure the hyperbolic progression in time of the average size of increments at varying scales, the progression of power versus frequency, or the progression of the variance of the wavelet coefficients at different scales [7], [8], [26]. A maximum likelihood fractal estimator was described in [20]. Recently, estimators for noisy fBm measurements that take advantage of the decorrelation effects of orthogonal wavelets were studied in [14], [33]. Deriche and Tewfik took advantage of the properties of the fdGn to devise a maximum likelihood estimator for the fdGn model [4]. Finally, an algorithm based on finding the fractal dimension of fBm by measuring the Lipshitz exponent (i.e. a singularity measurement) was presented in [13]. The decorrelation of adfGn by the discrete Haar transform and the algorithms for fBm estimation presented in [14], [33] motivates a simple parameter estimation algorithm which provides estimates of parameters ρ, H, and σ^2 of the adfGn model.

Suppose that given the input data, M scales of the Haar transform can be computed, and for each scale m, there are $N(m)$ Haar detail coefficients. Since the input data is assumed Gaussian (ESS processes are Gaussian by definition), the Haar coefficients are Gaussian. Then, using the assumption that the coefficients are uncorrelated, a log likelihood function based on the distribution of the wavelet coefficients is simply

$$L(\rho, H, \sigma^2) = -\frac{1}{2} \sum_{m=1}^{M} N(m) \left[\frac{\hat{\sigma}_m^2}{\sigma_m^2} + \log(2\pi\sigma_m^2) \right], \tag{4.4}$$

where $\hat{\sigma}_m^2$ is the sampled variance of the Haar coefficients at scale m and σ_m^2 is provided by (3.9)

for the adfGn growth function. Since the value of σ^2 that maximizes (4.4) for fixed ρ and H is

$$\sigma^2 = \frac{\sum_{m=1}^{M} N(m)\hat{\sigma}_m^2/\bar{\sigma}_m^2}{\sum_{m=1}^{M} N(m)}, \tag{4.5}$$

where $\bar{\sigma}_m^2$ is evaluated from (3.9) for $\sigma^2 = 1$, then (4.4) can reexpressed as a function of ρ and H. The parameter estimation algorithm is as follows. First, compute the Haar transform coefficients from the data sample. Then, calculate the sample variance of the coefficients at each scale, and maximize (4.4) (where (4.5) is substituted inside) over ρ and H by a steepest descent type of algorithm to obtain the estimates $\hat{\rho}$ and $\hat{H}$. Finally, obtain $\hat{\sigma}^2$ through (4.5). The attractive feature of this algorithm is that it requires no matrix inversion. The estimation algorithm for filtered fractal presented in [5] is an estimate-maximize (EM) algorithm that requires the inversion of a NxN matrix for every estimate step where N is the data length, and it can take many estimate steps for the EM algorithm to converge. The ESS models appear to provide a method to generalize fBm that provides faster algorithms than filtered fractals. Since the filtered fractal and adfGn models are different, the accuracy of the estimated parameters, however, cannot be directly compared.

4.3 Simulations

To test the estimation algorithm for the adfGn, we created 64 realizations of an adfGn of length 1024 samples with different parameters using the Cholesky decomposition technique [20], and we calculated estimates of H, ρ and σ^2. Table 1 shows the results with initial estimates $H = 1/2$ and $\rho = 0$ (white noise), and Table 2 shows the results when the initial estimates are the parameter values used to generate the test data. We see from Tables 1 and 2 that the descent algorithm finds equally good estimates with the two different initial conditions for most cases. However, the steepest descent algorithm could find the wrong local minimum with certain initial estimates in some cases. Obviously, further study is necessary to find a smart way to circumvent the problem that the likelihood function is not convex. It is also interesting to note that the algorithm can find a better estimate for H than ρ. One reason for this phenomena is that the fractal structure is consistent for all scales while the exponential structure dies out into the Brownian structure at coarser scales. In other words, the fractal structure carries more information at the larger scales. Over all, the performance of the proposed parameter estimation algorithm is good.

5 Conclusions and Extensions

The idea of extending the concept of self-similarity presents a much richer class of nonstationary process with stationary increments than fBm. The growth function concept provides new tools

for signal and image modeling. Since every discrete ESS process can be represented at the finest available scale by a stationary process with an otherwise arbitrary correlation function, one can use the growth function to create nonstationary (the ESS process) or stationary (the ESS increment) models. In this paper, one possible growth function using two parameters, i.e. ρ and H, was introduced to show how short term correlations can be added to the fBm model. The whitening property of the discrete Haar transform is useful for creating a fast parameter estimation algorithm for the new model.

The work on extend self-similarity is very preliminary, and many research problems can be studied in the future. A few of them are given below. First, we many consider to add more parameters to the signal model presented in Section 4 so that any finite order AR process can be represented. To achieve this objective, one possible stationary model is AR plus fBm. Unfortunately, using only the variance of the Haar coefficients for this problem will provide poor results because the AR part of the model behaves like white noise (i.e. $H = 1/2$) for large scales, and then problems arise because one would need to detect one fractal mode embedded in a second mode where $H = 1/2$ based on the wavelet coefficients for a small number of scales. Using the banded structure of the correlation matrix of the Haar coefficients may prove useful even though this would increase the complexity of the estimation algorithm. Second, the ESS models should be useful for texture synthesis and analysis. Since models that expand on fBm are possible, these new models will provide new features for better texture segmentation and provide more freedom for texture synthesis. The application of ESS to landscape modeling in computer graphics may help to increase the realism of fBm models. Third, methods to interpolate the growth function of discrete ESS to obtain a valid continuous growth function is of great interest. The interpolation method would allow for infinite resolution of textures and landscapes. Then, a user can zoom in arbitrarily into a computer generated mountain range that is not fractal at all scales. The signal models presented in Section 4 are only discrete ESS and the obvious continuous form of the growth function in (4.1) is not valid, and some kind of interpolation may be necessary for some applications. Fourth, an quantitative measure of roughness for ESS processes would be very valuable. In fact, the Hurst parameter already provides a roughness measure for the fBm model, and the rate of increase of the growth function should provide information about the visual level of roughness for the resulting ESS realizations. Finally, many multiresolution models exist for synthesis and analysis purposes and the ESS model is simply one of them. One multiresolution model is based the idea of considering processes that have an autoregressive (AR) structure on scale rather than time [1]. This new model has been applied for fast texture synthesis [19]. FBm models form a

subset of the new multiscale model under the assumption that the wavelet transform is the true KL transform for fBm so that a zeroth order (AR) process can generate the wavelet coefficients [32]. For good fBm synthesis, however, the KL approximation is limited. It is unclear if there is a basis that can transform ESS processes so that the coefficient of the basis are AR over scale. The connection between the new multiscale model and ESS model is still an open problem.

Appendices

A.1 Proof of Theorem 1

Through inspection of (2.5) with $H = 1/2$, it is easy to see that $r_{X_{1/2}}(k;\Delta x) = 0$ for $|k| > 0$, which means that the spectrum for dfGn with $H = 1/2$ has the following properties for all $\omega \in \mathbf{R}$,

$$S_{X_{1/2}}(e^{j\omega}) = C \quad \text{and} \quad S'_{X_{1/2}}(e^{j\omega}) = 0,$$

where C is a constant. The first statement of the theorem is proved. Differentiating (2.11) with respect to ω yields

$$\begin{aligned} S'_{X_H}(e^{j\omega}) &= K\left(\left[\frac{1/2\omega\cos(\omega/2) - (2H+1)\sin(\omega/2)}{\omega^{2H+2}}\right] + \left[\frac{1/2\cos(\omega/2)}{(2\pi-\omega)^{2H+1}} + \frac{(2H+1)\sin(\omega/2)}{(2\pi-\omega)^{2H+2}}\right]\right. \\ &\quad + \left[1/2\cos(\omega/2)\sum_{i=1}^{\infty}\frac{1}{(\omega+2\pi i)^{2H+1}} + \frac{1}{(-\omega+2\pi(i+1))^{2H+1}}\right] \\ &\quad \left. + \left[(2H+1)\sin(\omega/2)\sum_{i=1}^{\infty}\frac{1}{(-\omega+2\pi(i+1))^{2H+2}} - \frac{1}{(\omega+2\pi i)^{2H+2}}\right]\right), \\ S'_{X_H}(e^{j\omega}) &= T_1(H,\omega) + T_2(H,\omega) + T_3(H,\omega) + T_4(H,\omega), \end{aligned}$$

where K is a constant. With a little work it can be shown that for $H_1 > 1/2$, $H_2 < 1/2$, and $\omega \in (0,\pi]$ that

$$T_i(H_1,\omega) \le T_i(1/2,\omega) \le T_i(H_2,\omega) \quad \text{for } i = 1,\ldots,4,$$

and it follows that for $\omega \in (0,\pi]$,

$$S'_{X_{H_1}}(e^{j\omega}) \le 0 \le S'_{X_{H_2}}(e^{j\omega}).$$

The theorem follows. □

A.2 Validity of the Exponential Model

If the growth function has the form

$$f(s) = A(\rho^{|s|} - 1),$$

then the corresponding power spectrum obtained by taking the Fourier transform of (3.4) has a minimum value at $\omega = \pi$ of

$$S_f(e^{j\pi}) = -2A\frac{1-\rho}{1+\rho}.$$

Since the power spectrum of the ESS increments generated by a growth function of the form $f(s) = B|s|$ (i.e dfGn with $H = 1/2$) is $S_f(e^{j\omega}) = B$, then the increments of length Δx that are created from a growth function of the form of (3.11) have a power spectrum that possesses a minimum value at $\omega = \pi$ of

$$S_f(e^{j\pi}; \Delta x) = \frac{1}{(1-\rho)^2}\left[-4\rho\frac{1-\rho^{\Delta x}}{1+\rho^{\Delta x}} + (1-\rho^2)|\Delta x|\right].$$

It is enough to show that $S_f(e^{j\pi}; \Delta x) \geq 0$ for all Δx. It is easy to see that $S_f(e^{j\pi}; 0) = 0$ and that the derivative of $S_f(e^{j\pi}; \Delta x)$ with respect to Δx is

$$S'_f(e^{j\pi}; \Delta x) = \frac{1}{(1-\rho)^2}\left[\frac{\rho^{\Delta x}}{(1+\rho^{\Delta x})^2}8\rho\ln(\rho) + (1-\rho^2)\right],$$

which in turn has a minimum value at $\Delta x = 0$ of

$$S'_f(e^{j\pi}; 0) = \frac{1}{(1-\rho)^2}[2\rho\ln(\rho) + (1-\rho^2)].$$

Since it can be shown that $S'_f(e^{j\pi}; 0) \geq 0$ for all $0 \leq \rho \leq 1$, then $S'_f(e^{j\pi}; \Delta x) \geq 0$ and $S_f(e^{j\pi}; \Delta x) \geq 0$. Thus, the power spectrum of the increments of any length Δx is positive and (3.11) is a valid growth function for a continuous ESS process. □

A.3 Validity of AdfGn Model

Since the adfGn process is a discrete ESS process, it is enough to show that power spectrum of the increments where $\Delta x = 1$ is positive. The growth function (4.1) has a exponential term and a dfGn generating term with $1/2 < H < 1$. The contribution of the exponential term to the power spectrum has a minimum value at $\omega = \pi$ based upon the discussion in Appendix A.2. The dfGn term's contribution to the power spectrum has a minimum at $\omega = \pi$ by Theorem 1. Therefore the minimum value of the power spectrum of adfGn is

$$S_f(e^{j\pi}) = -\frac{2(A-1)}{1+|\rho|} + AS_{X_H}(e^{j\pi}),$$

where A and $S_{X_H}(e^{j\pi})$ is given by (4.2) and (2.11) with $\Delta x = 1$, respectively. If $-1 < \rho \leq 0$, then $A \leq 1$ and the power spectrum is positive. For $0 < \rho < 1$, to ensure that the short term correlations

are positive and that the power spectrum is positive, the A is constrained by

$$1 \leq A \leq \frac{2}{2 - S_{X_H}(e^{j\pi})(1+\rho)}.$$

One possible valid value for A is

$$A = \frac{2 - S_{X_H}(e^{j\pi}) + \rho S_{X_H}(e^{j\pi})}{2 - S_{X_H}(e^{j\pi}) - \rho S_{X_H}(e^{j\pi})}. \tag{A.1}$$

Under the approximation of (2.12), (A.1) becomes (4.2), and (4.1) would be a valid growth function for $-1 < \rho < 1$. It can be shown that, when (4.2) is chosen to represent A and $S_{X_H}(e^{j\pi})$ is approximated by (2.11), the actual bound $G(H)$ on ρ for a given H can be estimated by finding the smallest root of

$$(2-2H)S_{X_H}(e^{j\pi})\rho^2 + (8H - 8 + 2S_{X_H}(e^{j\pi}))\rho + 2HS_{X_H}(e^{j\pi}) = 0.$$

Note that (A.1) is not used for A in (4.1) because it does not have a closed form solution and a derivative would need to be calculated for the application of the steepest descent algorithm. For this reason, the linear approximation was chosen, and Fig. 1 does show that the linear approximation is a good estimate.

References

[1] M. Bassevile, A. Benveniste, K. C. Chou, S. A. Golden, R. Nikoukhah, and A. Willsky, "Modeling and estimation of multiresolution stochastic processes," *IEEE Trans. on Information Theory*, Vol. 38, pp. 766–784, Mar. 1992.

[2] C.-C. Chen, J. S. Daponte, and M. D. Fox, "Fractal feature analysis and classification in medical imaging," *IEEE Trans. on Medical Imaging*, pp. 133–142, June 1989.

[3] I. Daubechies, "Orthonormal bases of compactly supported wavelets," *Communications on Pure and Applied Mathematics*, Vol. 41, pp. 909–996, Nov. 1988.

[4] M. Deriche and A. H. Tewfik, "Maximum likelihood estimation of the parameters of discrete fractionally differenced gaussian noise processes." To appear in *IEEE Trans. on Signal Processing.*

[5] M. Deriche and A. H. Tewfik, "Signal modeling with filtered discrete fractional noise processes." To appear in *IEEE Trans. on Signal Processing.*

[6] P. Flandrin, "On the spectrum of fractional Brownian motions," *IEEE Trans. on Information Theory*, Vol. 35, pp. 197–199, Jan. 1989.

[7] P. Flandrin, "Wavelet analysis and synthesis of fractional Brownian motion," *IEEE Trans. on Information Theory*, Vol. 38, pp. 910–917, Mar. 1992.

[8] N. Gache, P. Flandrin, and D. Garreau, "Fractal dimension estimators for fractal Brownian motions," in *IEEE ICASSP-91*, pp. 3557–3560, Mar. 1991.

[9] I. S. Gradshteyn and I. M. Ryzhik, *Table of Integrals, Series, and Products*, New York, NY: Academic Press, 1980.

[10] C. W. Granger and R. Joyeux, "An introduction to long memory time series models and fractal differencing," *Journal of Time Series Analysis*, Vol. 1, No. 1, 1980.

[11] S. Hoefer, F. Heil, M. Pandit, and R. Kumaresan, "Segmentation of textures with different roughness using the model of isotropic two-dimensional fractional Brownian motion," in *IEEE ICASSP-93*, vol. 5, pp. 53–56, Apr. 1993.

[12] J. R. M. Hosking, "Fractional differencing," *Biometrika*, Vol. 68, No. 1, pp. 165–176, 1981.

[13] W.-L. Hwang, *Singularity detection, noise reduction and multifractal characterizaation using wavelets*, Ph.D. dissertation, New York University, 1993.

[14] L. M. Kaplan and C.-C. J. Kuo, "Fractal estimation from noisy data via discrete fractional Gaussian noise (dfGn) and the Haar basis." To appear in *IEEE Trans. on Signal Processing* (Special Issue on Wavelets).

[15] R. L. Kashyap and K.-B. Eom, "Texture boundary detection based on the long correlation model," *IEEE Trans. on Pattern Analysis and Machine Intelligence*, Vol. 11, pp. 58–67, Jan. 1989.

[16] R. L. Kashyap and P. M. Lapsa, "Synthesis and estimation of random fields using long-correlation models," *IEEE Trans. on Pattern Analysis and Machine Intelligence*, Vol. 6, pp. 800–809, Nov. 1984.

[17] M. S. Keshner, "$1/f$ noise," *Proceedings of the IEEE*, Vol. 70, pp. 212–218, Mar. 1982.

[18] J. P. Lewis, "Generalized stochastic subdivision," *ACM Trans. on Graphics*, Vol. 6, pp. 167–190, July 1987.

[19] M. R. Luettgen, W. C. Karl, A. S. Willsky, and R. R. Tenney, "Multiscale representations of Markov random fields." To appear in *IEEE Trans. on Signal Processing.*

[20] T. Lundahl, W. J. Ohley, S. M. Kay, and R. Siffert, "Fractional Brownian motion: A maximum likelihood estimator and its application to image texture," *IEEE Trans. on Medical Imaging*, Vol. 5, pp. 152–161, Sept. 1986.

[21] B. B. Mandelbrot, *The Fractal Geometry of Nature*, San Francisco, CA: Freeman, 1982.

[22] B. B. Mandelbrot and J. W. V. Ness, "Fractional Brownian motions, fractional noises and applications," *SIAM Review*, Vol. 10, pp. 422–437, Oct. 1968.

[23] E. Masry, "The wavelet transform of stochastic processes with stationary increments and its application to fractional Brownian motion," *IEEE Trans. on Information Theory*, Vol. 39, pp. 260–264, Jan. 1993.

[24] Y. Meyer, *Ondelettes et Operateurs*, Paris, France: Herman, 1990.

[25] H. O. Peitgen and D. Saupe, eds., *The Science of Fractal Images*, New York: Springer-Verlag, 1988.

[26] A. P. Pentland, "Fractal-based description of natural scenes," *IEEE Trans. on Pattern Analysis and Machine Intelligence*, Vol. 6, pp. 661–674, Nov. 1984.

[27] J. Ramanathan and O. Zeitouni, "On the wavelet transform of fractional Brownian motion," *IEEE Trans. on Information Theory*, Vol. 37, pp. 1156–1158, July 1991.

[28] W. Rudin, *Principles of Mathematical Analysis*, New York, NY: McGraw-Hill, 1976.

[29] A. H. Tewfik and M. Kim, "Fast multiscale statistical signal processing algorithms." To appear in *IEEE Trans. on Signal Processing.*

[30] A. H. Tewfik and M. Kim, "Correlation Structure of discrete wavelet coefficients of fractional Brownian motion," *IEEE Trans. on Information Theory*, Vol. 38, pp. 904–909, Mar. 1992.

[31] E. Wong, *Stochastic Processes in Information and Dynamical Systems*, New York, NY: McGraw-Hill, 1971.

[32] G. W. Wornell, "A Karhunen-Loève-like expansion for $1/f$ processes via wavelets," *IEEE Trans. on Information Theory*, Vol. 36, pp. 859–861, July 1990.

[33] G. W. Wornell and A. V. Oppenheim, "Estimation of fractal signals from noisy measurements using wavelets," *IEEE Trans. on Signal Processing*, Vol. 40, pp. 611–623, Mar. 1992.

Table Captions

Table 1: Means and standard deviations for the estimates of the parameters of adfGn where $\sigma^2 = 1$ and $H = 1/2$, $\rho = 0$ are the initial estimates.

Table 2: Means and standard deviations for the estimates of the parameters of adfGn where $\sigma^2 = 1$ and true parameters are the initial estimates.

Figure Captions

Figure 1: Estimate of the power spectrum of dfGN at $\omega = \pi$ versus H using (2.6) with the solid line and (2.11) with the dashed line.

Figure 2: A realization of the hyperbolic ESS process with $H = .65$ at scales $m = 4$ (top) and $m = 0$ (bottom).

Figure 3: A realization of the sinusoidal ESS process with $\omega = \pi/15$ at scales $m = 4$ (top) and $m = 0$ (bottom).

Figure 4: A realization of the exponential ESS process with $\rho = 0.85$ at scales $m = 4$ (top) and $m = 0$ (bottom).

Figure 5: The maximum possible value of ρ for a given value of H in the afBm model.

Figure 6: Comparison of the correlation for three different adfGn models with the same variance and same correlation at lag one.

Figure 7: A realiztion of afBm with $\rho = 0.85$ and $H = 0.65$ at scales $m = 4$ (top) and $m = 0$ (bottom).

Figure 8: Correlation decay of an adfGn process with $\rho = 0.5$ and $H = 0.75$.

Figure 9: Theoritical correlation matrix of the Haar wavelet coefficients of an adfGn process with $\rho = 0.5$ and $H = 0.75$.

Figure 10: Experimental correlation matrix of the Haar wavelet coefficients of an adfGn process with $\rho = 0.5$ and $H = 0.75$.

True Parameters		ρ		H		σ^2	
H	ρ	mean	std	mean	std	mean	std
.9	.5	.5187	.1539	.8809	.0749	1.1920	.8527
.9	0	-.0076	.2028	.8901	.0476	1.1205	.5711
.9	-.5	-.3458	.2435	.8756	.0377	0.9597	.2007
.7	.5	.4911	.0949	.6920	.0633	1.0142	.0772
.7	0	-.0283	.1578	.7020	.0477	1.0031	.0612
.7	-.5	-.2151	.2044	.6434	.0525	1.0007	.0454
.5	.5	.4419	.0585	.5465	.0828	1.0049	.0621
.5	0	-.0253	.1198	.5049	.0582	0.9978	.0379
.5	-.5	-.0479	.1632	.3452	.0885	0.9953	.0412

Table 1: Means and standard deviations for the estimates of the parameters of adfGn where $\sigma^2 = 1$ and $H = 1/2$, $\rho = 0$ are the initial estimates.

True Parameters		ρ		H		σ^2	
H	ρ	mean	std	mean	std	mean	std
.9	.5	.5186	.1403	.8839	.0575	1.1649	.8388
.9	0	-.0102	.1999	.8912	.0460	1.1232	.5704
.9	-.5	-.4056	.2417	.8824	.0379	0.9829	.2003
.7	.5	.5004	.0896	.6841	.0657	1.0094	.0780
.7	0	-.0287	.1583	.7021	.0479	1.0032	.0611
.7	-.5	-.4871	.1412	.6948	.0267	1.0070	.0464
.5	.5	.4813	.0374	.4929	.0494	1.0002	.0605
.5	0	-.0253	.1198	.5049	.0582	0.9978	.0379
.5	-.5	-.4627	.1688	.4795	.0540	0.9959	.0418

Table 2: Means and standard deviations for the estimates of the parameters of adfGn where $\sigma^2 = 1$ and true parameters are the initial estimates.

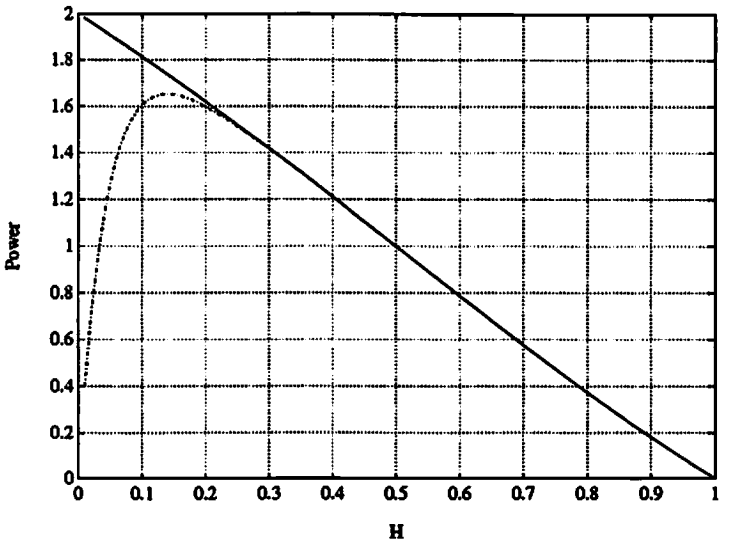

Figure 1: Estimate of the power spectrum of dfGN at $\omega = \pi$ versus H using (2.6) with the solid line and (2.11) with the dashed line.

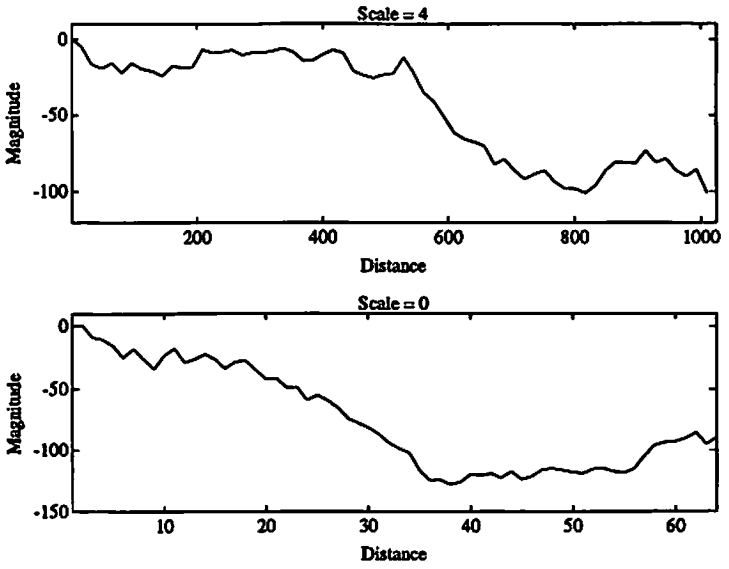

Figure 2: A realization of the hyperbolic ESS process with $H = .65$ at scales $m = 4$ (top) and $m = 0$ (bottom).

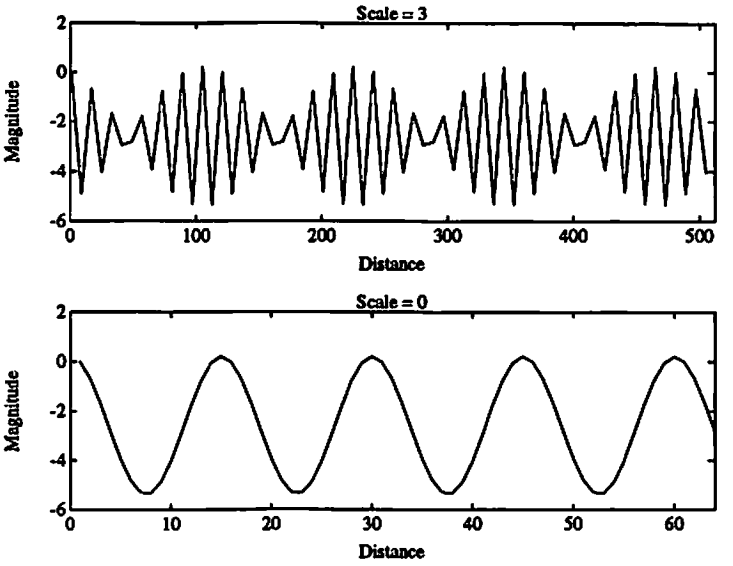

Figure 3: A realization of the sinusoidal ESS process with $\omega = \pi/15$ at scales $m = 4$ (top) and $m = 0$ (bottom).

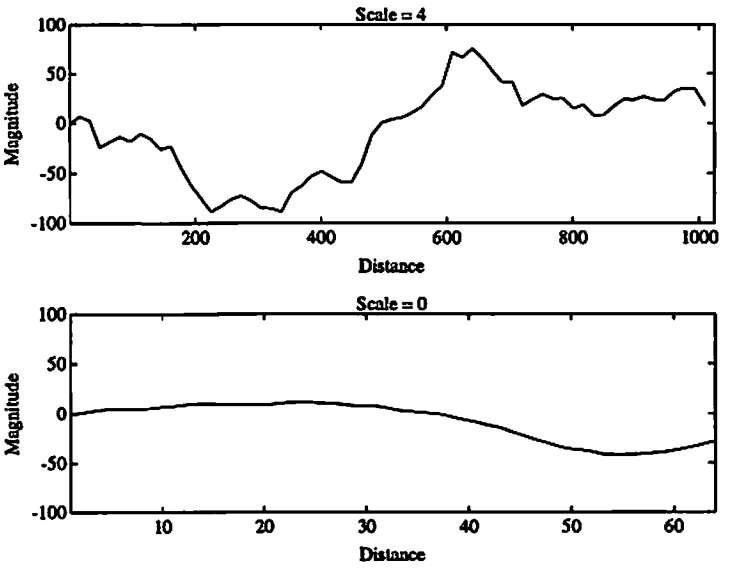

Figure 4: A realization of the exponential ESS process with $\rho = 0.85$ at scales $m = 4$ (top) and $m = 0$ (bottom).

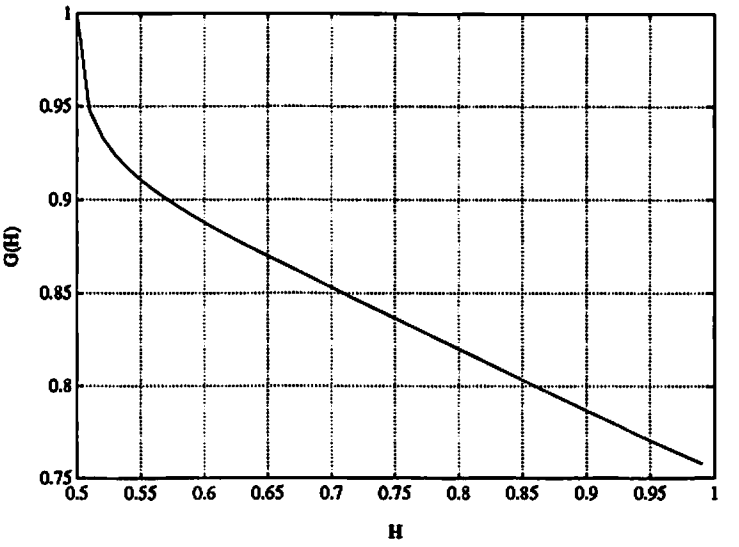

Figure 5: The maximum possible value of ρ for a given value of H in the afBm model.

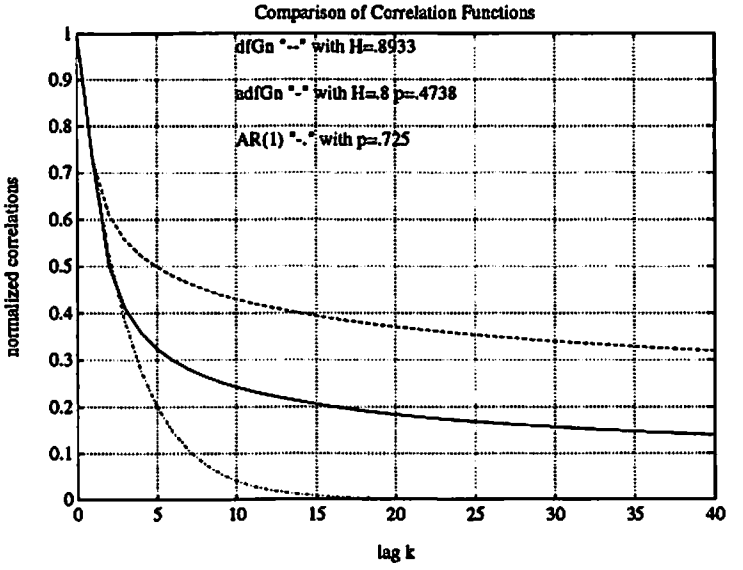

Figure 6: Comparison of the correlation for three different adfGn models with the same variance and same correlation at lag one.

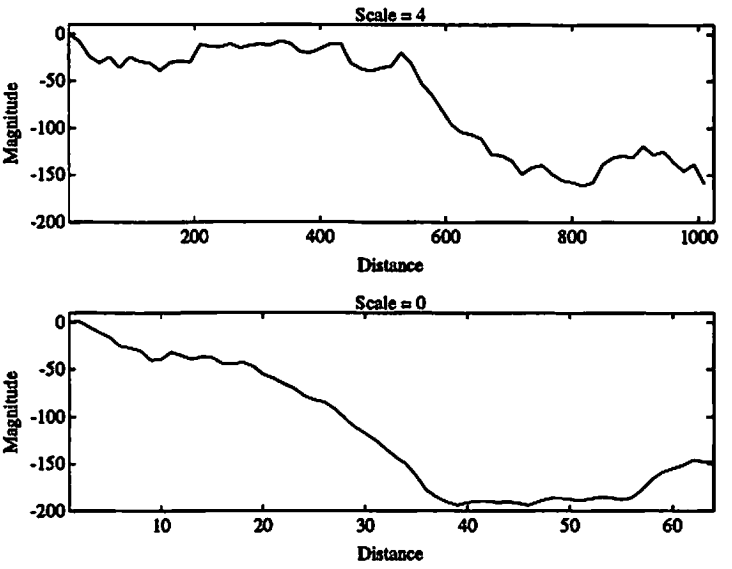

Figure 7: A realiztion of afBm with $\rho = 0.85$ and $H = 0.65$ at scales $m = 4$ (top) and $m = 0$ (bottom).

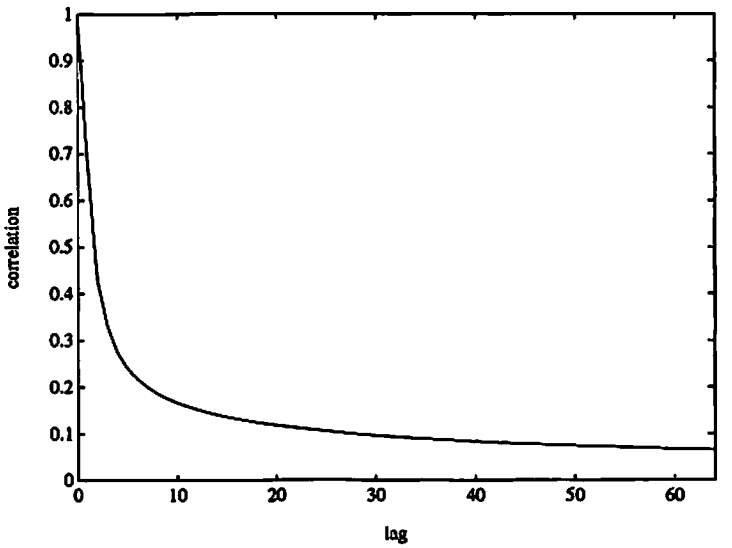

Figure 8: Correlation decay of an adfGn process with $\rho = 0.5$ and $H = 0.75$.

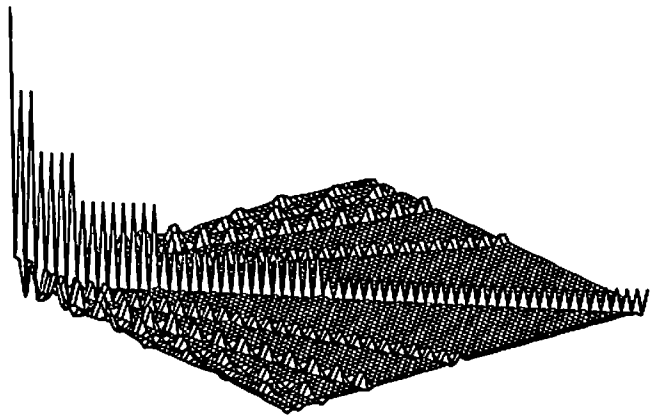

Figure 9: Theoritical correlation matrix of the Haar wavelet coefficients of an adfGn process with $\rho = 0.5$ and $H = 0.75$.

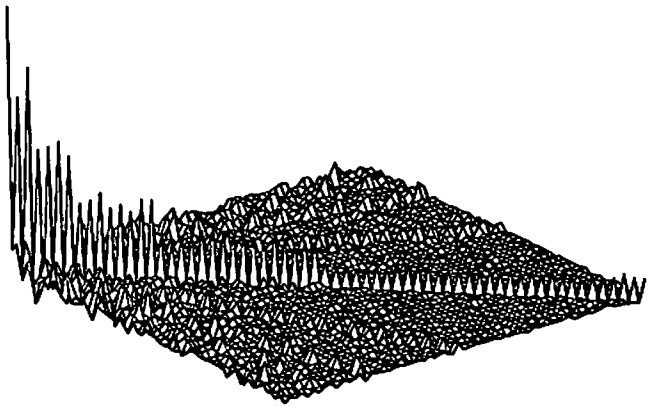

Figure 10: Experimental correlation matrix of the Haar wavelet coefficients of an adfGn process with $\rho = 0.5$ and $H = 0.75$.